energies

MDPI

Article

Multiscale Apparent Permeability Model of Shale Nanopores Based on Fractal Theory

Qiang Wang, Yongquan Hu, Jinzhou Zhao *, Lan Ren, Chaoneng Zhao and Jin Zhao

State Key Laboratory of Oil-Gas Reservoir Geology & Exploitation, Southwest Petroleum University, Chengdu 610500, China

* Correspondence: 201811000142@stu.swpu.edu.cn

Received: 4 August 2019; Accepted: 27 August 2019; Published: 2 September 2019

check for updates

Abstract: Based on fractal geometry theory, the Hagen–Poiseuille law, and the Langmuir adsorption law, this paper established a mathematical model of gas flow in nano-pores of shale, and deduced a new shale apparent permeability model. This model considers such flow mechanisms as pore size distribution, tortuosity, slippage effect, Knudsen diffusion, and surface extension of shale matrix. This model is closely related to the pore structure and size parameters of shale, and can better reflect the distribution characteristics of nano-pores in shale. The correctness of the model is verified by comparison with the classical experimental data. Finally, the influences of pressure, temperature, integral shape dimension of pore surface and tortuous fractal dimension on apparent permeability, slip flow, Knudsen diffusion and surface diffusion of shale gas transport mechanism on shale gas transport capacity are analyzed, and gas transport behaviors and rules in multi-scale shale pores are revealed. The proposed model is conducive to a more profound and clear understanding of the flow mechanism of shale gas nanopores.

Keywords: fractal; slippage effect; Knudsen diffusion; surface diffusion; apparent permeability

1. Introduction

Shale gas reservoirs have different reservoir formation modes and reservoir physical properties from conventional gas reservoirs, which leads to the complexity and multi-scale characteristics of shale gas percolation. Therefore, it is necessary to systematically analyze the gas migration mechanism in pore structures of different scales. Due to the nanoscale pore size of shale and the coexistence of multiple gas migration mechanisms, it is very challenging to simulate gas flow in the nanoscale pores of shale [1,2]. Most scholars have established the flow mathematical model and deduced the shale gas apparent permeability model mainly by dividing the flow pattern and considering the multiple migration mechanism of shale gas. Kuuskraa systematically analyzed the transport mechanism of shale gas and concluded that shale gas reservoirs are triple porous media. Shale gas transport mechanisms include gas desorption diffusion and Darcy flow. However, he did not propose a three-hole model considering multiple seepage mechanisms [3]. Roy and Raju defined the Knudsen number expression by using the average free path of gas molecules and pore radius of shale and other parameters, divided the flow of gas in shale pores into slip-off flow and transition flow, and believed that Darcy's flow law was not applicable to describe the gas migration of shale nanoscale pores [4]. Javadpour further established a mathematical model for gas flow considering diffusion and adsorption. By comparing this model with the conventional Darcy flow equation, the expression of apparent permeability is obtained [5]. This permeability can be applied directly to reservoir numerical simulation. It is shown that the ratio of apparent permeability to Darcy permeability increases with smaller pore size. Therefore, the influence of various migration mechanisms on the study of gas migration law of nano-pores in shale cannot be ignored. However, this theoretical model is based on the single-pipe model, without considering the actual complex pore structure of shale and the high-temperature and high-pressure characteristics of shale reservoir. Freeman established a multi-component fluid flow model based on micron-nanometer scale pore media by considering the interaction mechanism of convection, Knudsen diffusion and molecular diffusion [6]. In the same year, Curtis studied and described the structural characteristics of micron and nanometer shale by focusing ion beam and scanning electron microscope. The research results show that the physical characteristics of shale gas flow change with the change of pore radius, and the classic Darcy's law is no longer adaptive [7]. Under the pore size of shale observed by scanning electron microscope, it is necessary to consider the introduction of new flow mechanism when shale gas is transferred in reservoir. Ebrahim considered shale as a nano-pore medium, and proposed to study the flow of gas in nano-scale pore materials by using the Lattice Boltzmann method. It was believed that particle transport included the slippage of free gas molecules and the interfacial transport of adsorbed gas molecules. Studies show that there is a critical numeral, beyond which molecular slippage and interfacial transport may lead to the generation of molecular flow, which will improve the gas migration ability in the nanopores of organic matter [8]. Shabro considered slippage effect, Knudsen diffusion and adsorption and desorption, established pore scale seepage model, and quantitatively analyzed the contribution of Knudsen diffusion, adsorption and desorption to the whole flow. Studies show that slip flow and Knudsen diffusion have important effects on the apparent permeability of shale reservoirs. Gas desorption reduces shale reservoir pressure slowly, and slippage and Knudsen diffusion increase apparent permeability, which explains why actual production is higher than expected [9]. Michel modified Beskok and Karniadakis' equations to describe flow problems in nanoscale pores of shale reservoirs and extended the influence of arbitrary pore size distribution on apparent permeability under real gas conditions [10]. Freeman proposed a numerical model that can describe the porous size function of the diffusion and desorption process in shale. Combining macroscopic (reservoir fracture) and microscopic (diffusion of nanopores) physical phenomena, the model shows how gas composition varies over time and space during production [11]. Based on the research results of Javadpour and Swami and Settari established a single-tube flow model of shale gas in nanoscale pores by considering multiple seepage mechanisms such as Darcy flow, Knudsen diffusion and slippage effect. The finite difference method is used to solve the model, and the influence of Knudsen diffusion and slippage effect on gas production is analyzed and studied. The results show that the influence of the above factors on the production of shale gas reservoir must be taken into account [12,13]. Guo established the mathematical model of shale nano-pore seepage based on the convection-diffusion model, and deduced a new calculation formula of relative permeability. The reliability and accuracy of the model are verified by comparing with experimental data [14]. Singh ignored the slippage effect and derived the analytical formula of apparent permeability. The formula is only related to pore radius and pore morphology. It is considered that this model is applicable to all shale reservoir conditions where Knudsen number is less than 1 [15]. Mohammad et al. established the shale gas apparent permeability model based on gas dynamics principle. The results show that the gas molecular weight and temperature have significant effects on the apparent permeability, while the Tangential Momentum Accommodation Coefficient (TMAC) coefficient has the least effect. Through experimental study, it is found that there is no linear relationship between the apparent permeability and the adsorption concentration [16]. With the increase of the adsorption concentration, the influence of the adsorption concentration on the apparent permeability increases. Zhang established a new shale gas apparent permeability model by comprehensively considering slippage effect, Knudsen diffusion and surface diffusion, and verified it through experimental data. The research shows that when the local layer pressure decreases, the influence of surface diffusion on gas transportation in shale gradually increases, which cannot be ignored. When the local layer pressure is high, the effect of surface diffusion can be ignored [17]. Wang established a shale gas apparent permeability calculation model in real gas state by considering adsorption and desorption, stress sensitivity, non-Darcy effect and surface diffusion. Single-layer adsorption and multi-layer adsorption were described by uniform equation. The contributions of different flow mechanisms to apparent permeability and the sensitive parameters of apparent permeability are analyzed [18]. Wu established a model for calculating shale apparent permeability by considering the transport mechanism of free gas and air suction. It is considered that the total mass flux cannot be represented by the sum of Darcy flow mass flux and Knudsen diffusion mass flux, and the weight factors of Darcy flow mass flux and Knudsen diffusion mass flux are proposed based on the probability of molecular collision. The Langmuir isothermal adsorption equation and the material balance equation were used to calculate the apparent permeability [19]. Based on the fractal theory, Wang et al. deduced an analytical model for the apparent permeability of tight gas/shale gas under the conditions of gas convection and diffusion, and compared the experimental data to verify the accuracy of the model. But the flow characteristics of shale gas are not fully considered [20]. Wang et al. used logarithmic normal distribution function and cylindrical capillary to characterize pore size distribution in porous media and nanopores in matrix respectively, and proposed a real shale matrix pore gas transport model [21]. Zhang et al. established a random apparent liquid permeability model that considers the wettability and pore size related liquid slip effect, total organic carbon content, and the structural parameters. The results reveal the transport mechanism of dual wettability nano-porous shale [22]. Li et al. used the 3D intermingled-fractal model to derive a new permeability model for the organic-rich shale nanopore matrix and Shen et al. also developed an apparent permeability model of shale nanopores, which describes the adsorptive gas flow behavior in shale by considering the effects of gas adsorption, stress dependence, and non-Darcy flow [23,24]. In addition, there has been recent work showing that the constitutive equations of classical density functional theory, molecular dynamic simulations, Lattice Boltzmann and multi-continuum are able to reproduce more complex molecular dynamics simulations fluids in nanopores [25–28].

In previous studies on apparent permeability model in nano-pores of shale gas, the influences of pore structure, slippage effect, Knudsen diffusion and surface expansion on pore flow of shale matrix have not been comprehensively considered [29–31]. However, as shale reservoirs are different from conventional reservoirs in physical characteristics and gas occurrence characteristics, it is necessary to comprehensively consider each influencing factor when establishing flow mechanism. To achieve this goal, a new shale gas apparent permeability model is established based on fractal geometry theory, Hagen–Poiseuille law, and Langmuir adsorption law, which can be well matched with experimental data. This model integrates all characteristics of shale gas and is an important innovation in studying shale gas flow mechanism. This model can be a good reference for scientific research and engineering application.

2. Establishment of Multi-Scale Flow Mechanism of Shale Gas

2.1. Fractal Porous Media Model

Previous mathematical models of gas flow in shale matrix are based on the tortuous bundle model with uniform radius. However, the pore structure of shale matrix is extremely complex and random. The pore radius of shale is distributed at 0.3–300 nm [32], while the complex structure of matrix pores can be described by fractal geometry theory within a certain scale. Therefore, based on the fractal geometry theory, the tortuous bundle model with uneven pore radius distribution is adopted to characterize shale [19,33,34]. The physical model is shown in Figure 1.

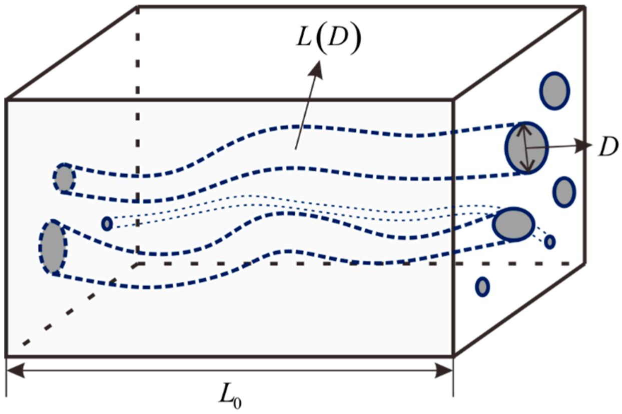

Figure 1. Shale tortuous bundle model.

The fractal porous media is composed of capillary bundles or pores with different sectional radii, and the tube radii of capillary bundles satisfy the fractal scale law, so the cumulative distribution of pore sizes in the unit section of the matrix is [35–38].

$$N(L \geq D) = \left(\frac{D_{\max}}{D}\right)^{D_p} \tag{1}$$

where N is the number of channels; L is the length scale; $D_{\max}$ is the pipe diameter of the largest capillary tube bundle, m; D is the fractal dimension of hole area.

Assuming that the distribution of pore size is continuous, the differential equation of pore diameter D in Equation (1) can be obtained

$$-dN = D_p D_{\max}^{D_p} D^{-(D_p+1)} dD \tag{2}$$

where $-dN > 0$ represents the cumulative number of pores increases with the decrease of pore diameter, so the total pore area on the flow section A_p is

$$A_p = -\int_{D_{\min}}^{D_{\max}} \frac{1}{4}\pi D^2 dN = \int_{D_{\min}}^{D_{\max}} \frac{1}{4}\pi D^2 D_p D_{\max}^{D_p} D^{-(D_p+1)} dD = \frac{\pi D_p D_{\max}^2}{4(2-D_p)}\left[1-\left(\frac{D_{\min}}{D_{\max}}\right)^{2-D_p}\right] \tag{3}$$

where $D_{\min}$ is the smallest capillary tube bundle pipe diameter, m.

Assuming that the porosity of the fractal porous media surface is equal to the volume porosity, the flow cross-sectional area (A) is

$$A = \frac{A_p}{\phi} = \frac{\pi D_p D_{\max}^2}{4\phi(2-D_p)}\left[1-\left(\frac{D_{\min}}{D_{\max}}\right)^{2-D_p}\right] \tag{4}$$

where ϕ is the porosity.

The relationship between length of tortuous capillary tube and radius of capillary tube can be expressed as fractal power law [39]:

$$L(D) = D^{1-D_t} L_0^{D_t} \tag{5}$$

where D_{t} is the fractal dimension of tortuosity; L_0 is the characteristic length of the capillary along the flow direction, m.

2.2. Shale Gas Multi-Scale Flow Model

Due to the random distribution of pore size in the shale matrix and different storage mechanisms (including viscous flow, free gas slip flow, transition flow and surface diffusion generated by adsorption and desorption) [25,40,41], there are multiple gas migration mechanisms in the shale reservoir, as shown in Figure 2.

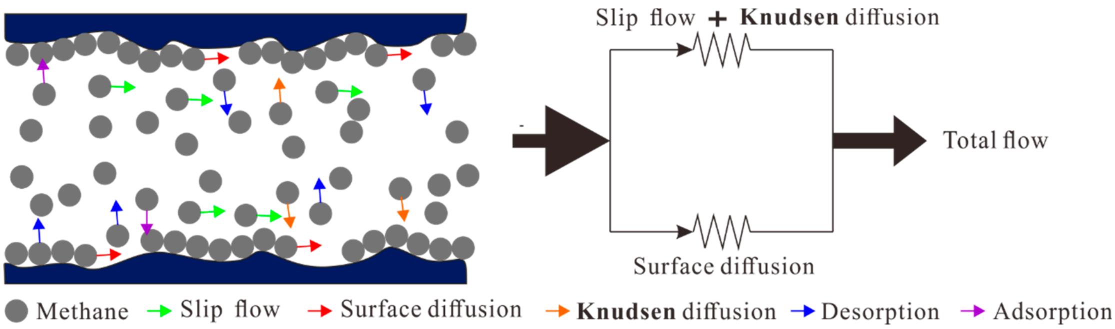

Figure 2. Multi-scale flow mechanism in shale nanopores.

2.2.1. Slip Flow

According to Hagen-Poiseuille law, the mass flux of mass flow through a single circular pipe cross section is [19,41,42]

$$J_{\mathrm{H}} = \frac{D^2 p M_{\mathrm{g}}}{32\mu ZRT}\frac{\Delta p}{L(D)} \tag{6}$$

where μ is gas viscosity, Pa·s; p is pore pressure, MPa; Z is the gas compression factor; R is the gas constant, 8.314 J/(mol·K); T is temperature, K; M_{g} is the molecular molar mass of the gas, kg/mol.

When K_{n} (Knudsen number) is between 0.001 and 0.1, the collision between gas molecules controls gas migration, and there is slippage effect. At this time, the flow state changes from viscous flow to slip flow, so Equation (6) needs to be corrected [43,44]. Considering the effects of slippage effect and rarefied gas effect, the expression of the mass flux (J_{H}) of the real gas flowing through the section of a single circular pipe after coefficient modification is

$$J_{\mathrm{H}} = (1+\alpha K_{\mathrm{n}})\left(1+\frac{4K_{\mathrm{n}}}{1-bK_{\mathrm{n}}}\right)\frac{D^2 p M_{\mathrm{g}}}{32\mu ZRT}\frac{\Delta p}{L(D)} \tag{7}$$

where

$$\alpha = \alpha_0 \frac{2}{\pi}\tan^{-1}\left(\alpha_1 K_{\mathrm{n}}^{\beta}\right) \tag{8}$$

where α is the effect coefficient of rarefied gas, dimensionless; b is the slip factor; is the effect coefficient of rarefied gas as the number approaches infinity, dimensionless; α_0 is the effect coefficient of rarefied gas as K_{n} approaches infinity, dimensionless; α_1, β is the fitting coefficient, dimensionless.

2.2.2. Knudsen Diffusion

When $10 \le K_{\mathrm{n}}$, the gas flow pattern is molecular free flow, and the gas mass flux (J_{N}) of a single circular tube under Knudsen diffusion is

$$J_{\mathrm{N}} = \frac{D}{3}\left(\frac{8M_{\mathrm{g}}}{\pi RT}\right)^{1/2}\frac{\Delta p}{L(D)} \tag{9}$$

By correcting Equation (9), the mass flux of real gas (J_{N}) through single circular pipe Knudsen diffusion is

$$J_{\mathrm{N}} = \frac{D}{3}C_{\mathrm{g}}\left(\frac{8ZM_{\mathrm{g}}}{\pi RT}\right)^{1/2}\frac{p}{Z}\frac{\Delta p}{L(D)} \tag{10}$$

where C_{g} is compression coefficient, MPa^{-1}.

A weighting factor was introduced to characterize the contribution rate of slip flux and Knudsen diffusion flux. The slip flow and Knudsen diffusion weighting factors were calculated by the ratio of the collision frequency between the gas molecules and the total collision frequency, and the ratio of collision frequency between gas molecules and nanopore wall to total collision frequency [19]. The relationship between the number of gas molecule collisions per unit time in nanopores is as follows

$$\frac{1}{t_T} = \frac{1}{t_M} + \frac{1}{t_S} \tag{11}$$

where t_T is the average time of gas molecules colliding once, s; t_M is the average time of one collision between gas molecules, s; t_S is the average time of a collision between gas molecules and nanopore wall, s.

The number of collisions can be expressed as

$$\frac{1}{t_T} = \frac{\overline{v}}{\lambda_T}\frac{1}{t_M} = \frac{\overline{v}}{\lambda}\frac{1}{t_S} = \frac{\overline{v}}{D} \tag{12}$$

where $\overline{v}$ is the average velocity of gas molecules, m/s; λ_T is the average free path of gas molecules, m; λ is the real gas mean free path, m.

Substitute Equation (12) into Equation (11) to get

$$\frac{1}{\lambda_T} = \frac{1}{\lambda} + \frac{1}{D} \tag{13}$$

The contribution of slip flow and Knudsen diffusion to free gas transport can be obtained by the ratio of the collision frequency between gas molecules and the total collision frequency, and the ratio of the collision frequency between gas molecules and the nanopore wall surface to the total collision frequency, respectively, then

$$\varepsilon_{\mathrm{H}} = \frac{1}{\lambda}/\frac{1}{\lambda_T} = \frac{1}{1+K_{\mathrm{n}}} \tag{14}$$

$$\varepsilon_{\mathrm{N}} = \frac{1}{D}/\frac{1}{\lambda_T} = \frac{1}{1+1/K_{\mathrm{n}}} \tag{15}$$

Then, the total mass flux of free gas through a single circular pipe cross section can be expressed as

$$J_{\mathrm{F}} = \varepsilon_{\mathrm{H}} J_{\mathrm{H}} + \varepsilon_{\mathrm{N}} J_{\mathrm{N}} \tag{16}$$

and the total mass flow rate of free gas through a single circular pipe section is

$$q_{\mathrm{F}}(D) = J_{\mathrm{F}}\frac{\pi D^2}{4}. \tag{17}$$

Substitute Equations (7), (10) and (16) into Equation (17) to get

$$q_{\mathrm{F}}(D) = \left(\varepsilon_{\mathrm{H}}(1+\alpha K_{\mathrm{n}})\left(1+\frac{4K_{\mathrm{n}}}{1-bK_{\mathrm{n}}}\right)\frac{D^2 p M_{\mathrm{g}}}{32\mu ZRT}\frac{\Delta p}{L(D)} + \varepsilon_{\mathrm{N}}\frac{D}{3}C_{\mathrm{g}}\left(\frac{8ZM_{\mathrm{g}}}{\pi RT}\right)^{1/2}\frac{p}{Z}\frac{\Delta p}{L(D)}\right)\frac{\pi D^2}{4}. \tag{18}$$

By integrating the total mass flow rate of free gas through single circular pipe section in the interval of minimum pore diameter and maximum pore diameter $[D_{\mathrm{min}}, D_{\mathrm{max}}]$, the total mass flow rate of free gas in shale gas porous media can be obtained

$$\begin{aligned} Q_{\mathrm{F}}(D) &= -\int_{D_{\mathrm{min}}}^{D_{\mathrm{max}}} q_{\mathrm{F}}(D) dN \\ &= \int_{D_{\mathrm{min}}}^{D_{\mathrm{max}}} \left(\varepsilon_{\mathrm{H}}(1+\alpha K_{\mathrm{n}})\left(1+\frac{4K_{\mathrm{n}}}{1-bK_{\mathrm{n}}}\right)\frac{D^2 p M_{\mathrm{g}}}{32\mu ZRT}\frac{\Delta p}{L(D)} + \varepsilon_{\mathrm{N}}\frac{D}{3}C_{\mathrm{g}}\left(\frac{8ZM_{\mathrm{g}}}{\pi RT}\right)^{1/2}\frac{p}{Z}\frac{\Delta p}{L(D)}\right)\frac{\pi D^2}{4} D_p D_{\mathrm{max}}^{D_p} D^{-(D_p+1)} dD \\ &= \frac{\pi}{4}\frac{p}{Z}\frac{D_p D_{\mathrm{max}}^{D_p}\Delta p}{L_0^{D_t}}\int_{D_{\mathrm{min}}}^{D_{\mathrm{max}}}\left(\varepsilon_{\mathrm{H}}(1+\alpha K_{\mathrm{n}})\left(1+\frac{4K_{\mathrm{n}}}{1-bK_{\mathrm{n}}}\right)\frac{M_{\mathrm{g}}}{32\mu ZRT} D^{2-D_p+D_t} + \varepsilon_{\mathrm{N}}\frac{1}{3}C_{\mathrm{g}}\left(\frac{8ZM_{\mathrm{g}}}{\pi RT}\right)^{1/2} D^{1-D_p+D_t}\right) dD \end{aligned} \tag{19}$$

2.2.3. Adsorption and Desorption

In the pressure attenuation process of shale gas reservoir exploitation, shale gas adsorption and desorption is a very fast physical process compared with surface diffusion, so the adsorption amount can be calculated by Langmuir's adsorption law

$$q_{\mathrm{ai}} = \frac{q_L p}{p_L + p} \tag{20}$$

where q_L is Langmuir volume, m^3/kg; p_L is Langmuir pressure, MPa.

Considering the influence of real gas, the adsorption capacity is

$$q_{\mathrm{a}} = \frac{q_L p/Z}{p_L + p/Z} \tag{21}$$

Gas coverage was defined as the ratio of adsorbed gas volume to Langmuir volume, and the gas coverage of ideal gas and real gas was respectively

$$\theta_{\mathrm{i}} = \frac{p}{p_L + p} \tag{22}$$

$$\theta = \frac{p/Z}{p_L + p/Z} \tag{23}$$

where θ_{i} is the gas coverage of ideal gas, dimensionless; θ is the gas coverage of real gas, dimensionless.

Due to the adhesion of adsorbed gas molecules to the pore surface, the nano-pore space of shale decreases, and the effective diameter of ideal gas and real gas flow is

$$D_{\mathrm{ei}} = D - 2d_{\mathrm{m}}\theta_{\mathrm{i}} \tag{24}$$

$$D_{\mathrm{e}} = D - 2d_{\mathrm{m}}\theta \tag{25}$$

where d_{m} is the molecular diameter of methane, m.

2.2.4. Surface Diffusion

In shale gas, the concentration of adsorbed gas is much higher than that of free gas. Due to the adsorption and desorption of shale gas, the influence of surface diffusion on gas migration cannot be ignored. The mass flux (J_{B}) under the surface diffusion of a single circular pipe can be expressed as

$$J_{\mathrm{B}} = D_{\mathrm{B}}^{0} \frac{C_{\mathrm{sc}}}{p} \frac{\Delta p}{L(D)} \tag{26}$$

where C_{sc} is the adsorption gas concentration, kg/m^3; D_{B}^{0} is the surface diffusion coefficient when gas coverage is 0.

According to Chen and Yang, the surface diffusion coefficient considering gas coverage is [45]

$$D_{\mathrm{B}} = D_{\mathrm{B}}^{0} \frac{(1-\theta) + \frac{\kappa}{2}\theta(2-\theta) + [H(1-\kappa)](1-\kappa)\frac{\kappa}{2}\theta^2}{\left(1-\theta+\frac{\kappa}{2}\theta\right)^2} \tag{27}$$

where

$$H(1-\kappa) = \begin{cases} 0 & \kappa \geq 1 \\ 10 & \leq \kappa < 1 \end{cases} \tag{28}$$

Combined with Equations (22) and (23), the ideal adsorbed gas concentration and the real adsorbed gas concentration in Langmuir monolayer adsorbed shale nano-pores are respectively expressed as

$$C_{\mathrm{sci}} = \frac{4\theta_{\mathrm{i}} M_{\mathrm{g}}}{\pi d_{\mathrm{m}}^3 N_{\mathrm{A}}} \tag{29}$$

$$C_{\mathrm{sc}} = \frac{4\theta M_{\mathrm{g}}}{\pi d_{\mathrm{m}}^3 N_{\mathrm{A}}} \tag{30}$$

where κ is the diffusion capacity coefficient of gas molecules; θ is the true gas hole wall coverage; N_{A} is Avogadro constant, 6.022×10^{23} mol^{-1}.

By introducing Equations (29) and (30) into Equation (26), the mass flux under surface diffusion of desired (J_{Bi}) and real (J_{B}) adsorbed gas can be expressed as follows

$$J_{\mathrm{Bi}} = D_{\mathrm{B}}^0 \frac{4\theta_{\mathrm{i}} M_{\mathrm{g}}}{\pi d_{\mathrm{m}}^3 N_{\mathrm{A}} p} \frac{\Delta p}{L(D)} \tag{31}$$

$$J_{\mathrm{B}} = D_{\mathrm{B}} \frac{4\theta M_{\mathrm{g}}}{\pi d_{\mathrm{m}}^3 N_{\mathrm{A}} p} \frac{\Delta p}{L(D)} \tag{32}$$

In real state, the surface diffusion mass flow rate of adsorbed gas through single circular pipe section is

$$q_{\mathrm{B}}(D) = D_{\mathrm{B}} \frac{4\theta M_{\mathrm{g}}}{\pi d_{\mathrm{m}}^3 N_{\mathrm{A}} p} \frac{\Delta p}{L(D)} \frac{\pi D^2}{4} \tag{33}$$

By integrating the mass flow rate of adsorbed gas diffusing on the surface of single circular pipe section in the interval of minimum pore diameter and maximum pore diameter $[D_{\mathrm{min}}, D_{\mathrm{max}}]$, the mass flow rate of adsorbed gas diffusing on the surface of shale fractal porous media is

$$\begin{aligned} Q_{\mathrm{B}}(D) &= \int_{D_{\mathrm{min}}}^{D_{\mathrm{max}}} D_{\mathrm{B}} \frac{4\theta M_{\mathrm{g}}}{\pi d_{\mathrm{m}}^3 N_{\mathrm{A}} p} \frac{\Delta p}{D^{1-D_t} L_0^{D_t}} \frac{\pi D^2}{4} D_p D_{\mathrm{max}}^{D_p} D^{-(D_p+1)} dD \\ &= D_{\mathrm{B}} \frac{\theta M_{\mathrm{g}}}{d_{\mathrm{m}}^3 N_{\mathrm{A}} p} \frac{\Delta p}{L_0^{D_{\mathrm{t}}}} \frac{D_p D_{\mathrm{max}}^{D_p}}{1-D_p+D_t} \left(D_{\mathrm{max}}^{1-D_p+D_t} - D_{\mathrm{min}}^{1-D_p+D_t} \right) \end{aligned} . \tag{34}$$

2.3. Apparent Shale Gas Permeability

Gas migration mechanism in nanoscale pores of shale matrix includes free gas slip flow, Knudsen diffusion and surface diffusion of adsorbed gas, so the total mass flow rate of gas flowing through nanoscale pores of shale matrix is

$$Q = Q_{\mathrm{F}} + Q_{\mathrm{B}} \tag{35}$$

According to Darcy's law, the mass flow rate of porous media is expressed as

$$Q = \frac{K_{\mathrm{app}} A}{\mu} \frac{p M_{\mathrm{g}}}{ZRT} \frac{\Delta p}{L_0} \tag{36}$$

By substituting Equations (19), (34), and (35) into Equation (36), the apparent shale permeability under various flow mechanisms can be written as

$$\begin{aligned} K_{\mathrm{app}} &= \frac{\mu RT}{M_{\mathrm{g}}} \frac{\phi(2-D_p)}{L_0^{D_t-1}\left(D_{\mathrm{max}}^{2-D_p} - D_{\mathrm{min}}^{2-D_p}\right)} \int_{D_{\mathrm{min}}}^{D_{\mathrm{max}}} \left(\varepsilon_{\mathrm{H}} (1+\alpha K_{\mathrm{n}}) \left(1 + \frac{4K_{\mathrm{n}}}{1-bK_{\mathrm{n}}}\right) \frac{M_{\mathrm{g}}}{32\mu RT} D^{2-D_p+D_t} + \varepsilon_{\mathrm{N}} \frac{C_{\mathrm{g}}}{3} \left(\frac{8ZM_{\mathrm{g}}}{\pi RT}\right)^{1/2} D^{1-D_p+D_t} \right) dD \\ &+ \mu D_{\mathrm{B}} \frac{\theta ZRT}{d_{\mathrm{m}}^3 N_{\mathrm{A}} p^2} \frac{D_{\mathrm{max}}^{1-D_p+D_t} - D_{\mathrm{min}}^{1-D_p+D_t}}{L_0^{D_t-1}(1-D_p+D_t)} \frac{4\phi(2-D_p)}{\pi\left(D_{\mathrm{max}}^{2-D_p} - D_{\mathrm{min}}^{2-D_p}\right)} \end{aligned} \tag{37}$$

By integrating and differentiating Equation (37), the analytical formula of apparent permeability can be obtained as follows:

$$\begin{aligned}K_{\text{app}} &= \frac{\mu RT}{M_{\text{g}}}\frac{\phi(2-D_p)}{L_0^{D_t-1}\left(D_{\max}^{2-D_p}-D_{\min}^{2-D_p}\right)}\left(\begin{array}{c}\frac{\varepsilon_{\text{H}}}{3-D_p+D_t}\frac{M_{\text{g}}}{32\mu RT}(1+\alpha K_{\text{n}})\left(1+\frac{4K_{\text{n}}}{1-bK_{\text{n}}}\right)\left(D_{\max}^{3-D_p+D_t}-D_{\min}^{3-D_p+D_t}\right)\\ +\frac{\varepsilon_{\text{N}}}{2-D_p+D_t}\frac{C_{\text{g}}}{3}\left(\frac{8ZM_{\text{g}}}{\pi RT}\right)^{1/2}\left(D_{\max}^{2-D_p+D_t}-D_{\min}^{2-D_p+D_t}\right)\end{array}\right)\\ &+\mu D_{\text{B}}\frac{\theta ZRT}{d_{\text{m}}^3N_{\text{A}}p^2}\frac{D_{\max}^{1-D_p+D_t}-D_{\min}^{1-D_p+D_t}}{L_0^{D_t-1}(1-D_p+D_t)}\frac{4\phi(2-D_p)}{\pi\left(D_{\max}^{2-D_p}-D_{\min}^{2-D_p}\right)}\end{aligned} \quad (38)$$

It can be seen from Equation (38) that the apparent permeability of shale considering multiple gas migration mechanism is composed of three parts, which can be respectively regarded as the apparent permeability of slip flow (K_{H}), the apparent permeability of Knudsen diffusion (K_{N}) and the apparent permeability of surface diffusion (K_{B}). The form can be expressed as

$$K_{\text{H}} = \frac{1}{32}(1+\alpha K_{\text{n}})\left(1+\frac{4K_{\text{n}}}{1-bK_{\text{n}}}\right)\frac{\phi\varepsilon_{\text{H}}}{L_0^{D_t-1}}\frac{2-D_p}{3-D_p+D_t}\frac{D_{\max}^{3-D_p+D_t}-D_{\min}^{3-D_p+D_t}}{D_{\max}^{2-D_p}-D_{\min}^{2-D_p}} \quad (39)$$

$$K_{\text{N}} = \frac{\mu C_{\text{g}}}{3}\left(\frac{8ZM_{\text{g}}}{\pi RT}\right)^{1/2}\frac{\phi\varepsilon_{\text{N}}}{L_0^{D_t-1}}\frac{2-D_p}{2-D_p+D_t}\frac{D_{\max}^{2-D_p+D_t}-D_{\min}^{2-D_p+D_t}}{D_{\max}^{2-D_p}-D_{\min}^{2-D_p}} \quad (40)$$

$$K_{\text{B}} = 4\mu D_{\text{B}}\frac{\theta ZRT}{\pi d_{\text{m}}^3N_{\text{A}}p^2}\frac{\phi}{L_0^{D_t-1}}\frac{2-D_p}{1-D_p+D_t}\frac{D_{\max}^{1-D_p+D_t}-D_{\min}^{1-D_p+D_t}}{D_{\max}^{2-D_p}-D_{\min}^{2-D_p}} \quad (41)$$

Through Equations (39)–(41), the relationship between slip apparent permeability, Knudsen diffusion apparent permeability, surface diffusion apparent permeability and geometric fractal parameters is established, and the relationship between matrix apparent permeability of shale gas reservoir and three flow mechanisms and geometric fractal theory is also established through Equation (38).

According to fractal geometry theory and Darcy flow equation, Darcy permeability (K_D) of shale can also be obtained as

$$K_D = \frac{\pi D_p D_{\max}^{D_p}\left(D_{\max}^{3-D_p+D_t}-D_{\min}^{3-D_p+D_t}\right)}{128L_0^{D_t-1}A\left(3-D_p+D_t\right)} = \frac{1}{32}\frac{\phi}{L_0^{D_t-1}}\frac{2-D_p}{D_{\max}^{2-D_p}-D_{\min}^{2-D_p}}\frac{D_{\max}^{3+D_t-D_p}-D_{\max}^{3+D_t-D_p}}{3+D_t-D_p} \quad (42)$$

Equations (38)–(42) contain many parameters. Among them, porosity, physical parameters of shale gas, temperature, and diameter of maximum and minimum capillary bundle are all obtained by experimental methods. Fractal dimension (D_p and D_t) can be referred to Yu's study [35]. The value of Knudsen's number is obtained by Equation (49).

3. Model Validation

Firstly, fractal characterization of shale pore characteristics is needed to obtain integral shape dimension of shale pore surface and fractal dimension of pore tortuosity. According to the 2D model proposed by Yu et al. [35], the relationship between the integral shape dimension of the pore surface and the distribution of pore size is

$$D_p = 2 - \frac{\ln\phi}{\ln(D_{\min}/D_{\max})} \quad (43)$$

It is noteworthy that Equation (46) needs to satisfy the precondition of $D_{\min}/D_{\max} < 0.01$, which is obviously satisfied in shale reservoirs. Because the fractal dimension of pore tortuosity of shale has not yet been measured, the fractal dimension of pore tortuosity is determined by the model proposed by Yu et al. [35].

$$D_t = 1 + \frac{\ln \tau_{\mathrm{av}}}{\ln(L_0/D_{\mathrm{av}})} \tag{44}$$

where τ_{av} is the average tortuosity, dimensionless; D_{av} is the average pore diameter, m.

The shale permeability test data of Letham et al. were used for model verification [46]. In its experimental test, helium and methane were used to measure shale permeability, and the basic input parameters of model verification were shown in Table 1.

Table 1. Basic input parameters of the shale apparent permeability model.

Parameters	Value	Unit
Minimum pore diameter	0.4	nm
Maximum pore diameter	100	nm
Temperature	303	K
Langmuir pressure	5	MPa
Gas constant	8.314	J/(mol·K)
Avogadro constant	6.022×10^{23}	Mol^{-1}

Since gas viscosity is a function of pressure, the widely used formula is adopted to calculate, namely [47–50]

$$\mu = 10^{-4} H_0 \exp\left[X\left(10^{-3}\frac{28.96\gamma_{\mathrm{g}} p}{ZRT}\right)^{0.2(12-X)}\right] \tag{45}$$

$$X = 0.01\left(350 + \frac{54777.78}{T} + 28.96\gamma_{\mathrm{g}}\right) \tag{46}$$

$$H_0 = \frac{\left(9.379 + 0.01607\gamma_{\mathrm{g}}\right)T^{1.5}}{209.2 + 19.26\gamma_{\mathrm{g}}} \tag{47}$$

where γ_{g} is gas molar weight, kg/mol.

Since shale has no adsorption effect on helium gas, the effect of surface diffusion on apparent permeability is not considered when calculating the apparent permeability of helium gas. At this time, the expression of apparent permeability is simplified as

$$K_{\mathrm{app}} = \frac{\mu RT}{M_{\mathrm{g}}} \frac{\phi(2-D_p)}{L_0^{D_t-1}\left(D_{\max}^{2-D_p} - D_{\min}^{2-D_p}\right)} \left(\begin{array}{l} \frac{\varepsilon_{\mathrm{H}}}{3-D_p+D_t} \frac{M_{\mathrm{g}}}{32\mu RT}(1+\alpha K_{\mathrm{n}})\left(1+\frac{4K_{\mathrm{n}}}{1-bK_{\mathrm{n}}}\right)\left(D_{\max}^{3-D_p+D_t} - D_{\min}^{3-D_p+D_t}\right) \\ + \frac{\varepsilon_{\mathrm{N}}}{2-D_p+D_t} \frac{C_{\mathrm{g}}}{3}\left(\frac{8ZM_{\mathrm{g}}}{\pi RT}\right)^{1/2}\left(D_{\max}^{2-D_p+D_t} - D_{\min}^{2-D_p+D_t}\right) \end{array}\right) \tag{48}$$

As can be seen from Figure 3, the calculated results of the model in this paper are very close to the experimental data. The apparent permeability of shale ranges from 400 nD to 1300 nD, and decreases with the increase of pressure. This is because with the decrease of pressure, the molecular mean free path increases and the K_{n} number increases, the influence of microscopic seepage on permeability increases, and the deviation from Darcy permeability increases. In addition, under the same reservoir conditions, even if the apparent permeability of methane is contributed by surface diffusion, the apparent permeability of helium is always greater than the apparent permeability of methane. It can be explained that the collision radius of helium molecule (0.26 nm) is smaller than that of methane molecule (0.38 nm), so the helium K_{n} number is larger than methane K_{n} number, and the apparent permeability is higher. The following formula can be used for calculating K_{n} number [51]:

$$K_{\mathrm{n}} = \frac{\mu}{pD}\sqrt{\frac{\pi ZRT}{2M_{\mathrm{g}}}} \tag{49}$$

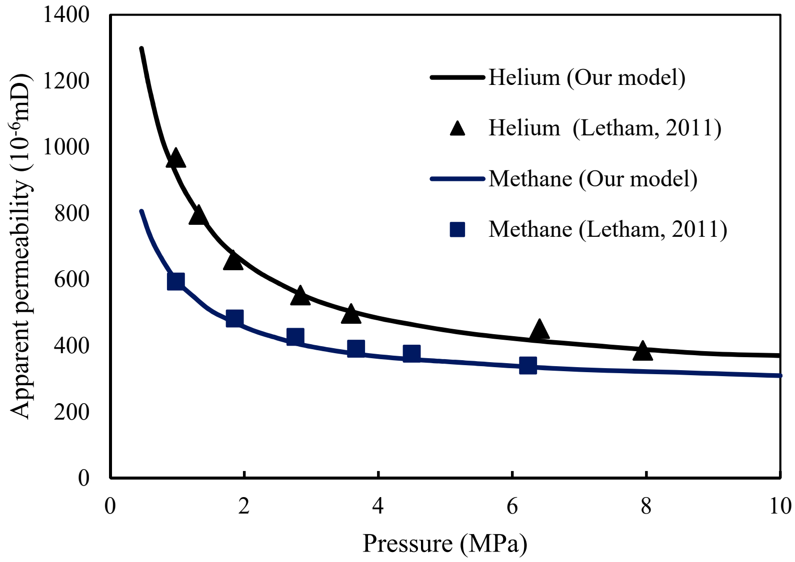

Figure 3. Comparison of apparent permeability calculated by the model in this paper with experimental data.

4. Discussion of Results

Based on fractal theory, this paper establishes a shale nano-pore permeability model considering the integral shape dimension of pore surface, fractal dimension of tortuosity, surface diffusion, Knudsen diffusion and slip flow. Based on the parameters in Table 2, we analyzed the apparent permeability and the contribution rate of different components to the apparent permeability. These results are of great significance to the study of microscopic seepage mechanism of nano-pore shale gas.

Table 2. Basic input parameters of the shale apparent permeability model.

Parameters	Value	Unit
Minimum pore diameter	1	nm
Maximum pore diameter	100	nm
Temperature	350	K
Langmuir pressure	5	MPa
Gas constant	8.314	J/(mol·K)
Avogadro constant	6.022×10^{23}	Mol^{-1}
Tortuosity	5	
Porosity	3	%
Surface diffusion coefficient	1×10^{-7}	m/s^2
Gas viscosity	0.015	mPa·s

The variation trend of various dimensionless apparent permeability with pressure is shown in Figure 4. As can be seen from the Figure 4, slip flow permeability, Knudsen diffusion permeability, surface diffusion permeability and apparent permeability all decrease with the increase of pressure. When the pressure increases, the average free path of gas molecules decreases, and the gas flow under the action of slip flow, Knudsen diffusion and surface diffusion (from Equation (40)) decreases. Therefore, the permeability decreases. When the pressure is less than 10 MPa, the slip flow permeability, surface diffusion permeability and apparent permeability rapidly decrease with the increase of pressure, and then tend to flatten. Therefore, under low pressure, pressure has a great influence on the apparent permeability of shale, while under high pressure, pressure has a relatively small influence on the apparent permeability. In essence, these performances can explain the phenomenon that in shale gas production, with the decrease of reservoir pressure, the apparent permeability gradually increases, and the rate of production decline gradually decreases. The effect of temperature on dimensionless apparent permeability is shown in Figure 5. The dimensionless apparent permeability increases nonlinearly with temperature.

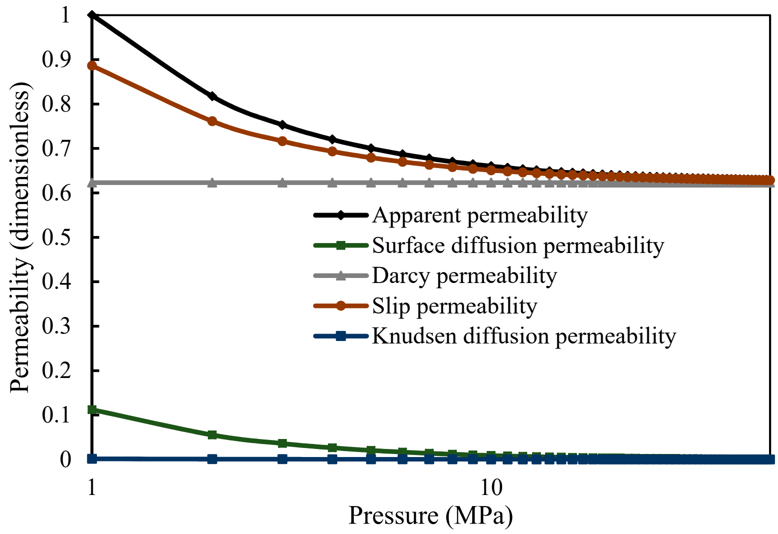

Figure 4. Relationship between dimensionless permeability and pressure.

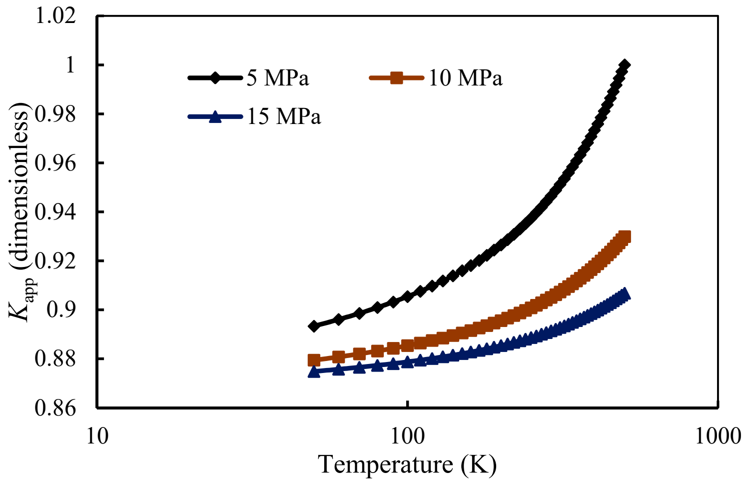

Figure 5. Relationship between temperature and dimensionless apparent permeability.

The contribution rates of different gas migration mechanisms to apparent permeability (K_{app}) are shown in Figure 6. It can be seen from the figure that the slip flow contributes the most to the apparent permeability, followed by the surface diffusion ($k_B = K_B/K_{app}$), and finally the Knudsen diffusion ($k_N = K_N/K_{app}$). The contribution rate of slip flow ($k_H = K_H/K_{app}$) to apparent permeability increases rapidly and then tends to flatten with the increase of pressure, while the contribution rate of surface diffusion to apparent permeability decreases rapidly and then tends to flatten with the increase of pressure. Under low pressure, the contribution of surface diffusion to apparent permeability is more significant, but even at pressure of 1 MPa, it is less than 10%. The contribution of slip flow to the apparent permeability is dominant, while the contribution of Knudsen diffusion to the apparent permeability is small, which can be ignored.

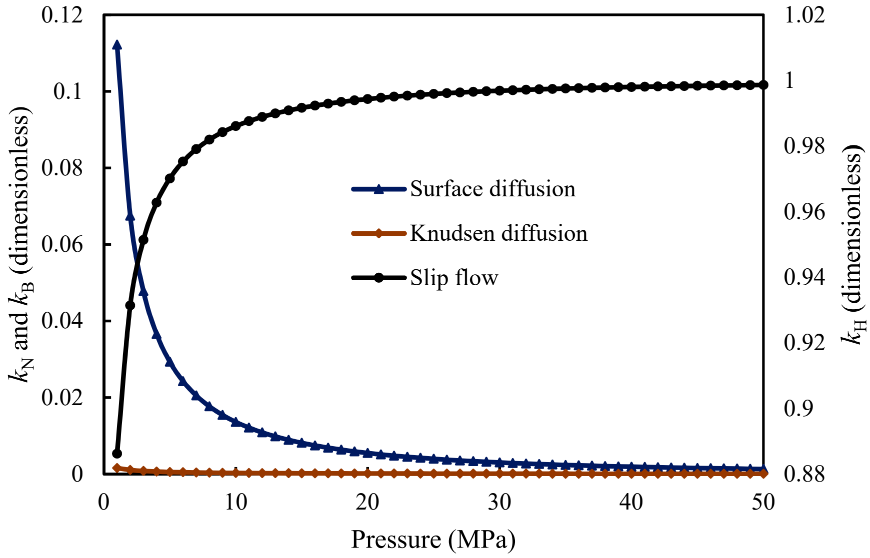

Figure 6. Relationship between contribution rate and pressure.

The overall effect of fractal dimension on dimensionless apparent permeability is shown in Figure 7. The apparent permeability increases with the increase of the integral shape dimension of the pore surface, and the change relation is strongly nonlinear. The relationship between tortuosity fractal dimension and apparent permeability is linearly negative. The influences of the integral shape dimension of pore surface and the fractal dimension of tortuosity on the contribution rate of permeability of different mechanisms are shown in Figures 8 and 9. Figure 8 shows that the surface diffusion contribution rate (k_B) and Knudsen diffusion contribution rate (k_N) are positively correlated with the integral shape dimension of the pore surface, while the slip flow is negatively correlated with the integral shape dimension of the pore surface. The integral shape dimension of the pore surface has the least effect on Knudsen diffusion. However, the influence of fractal dimension of tortuosity on contribution rate is opposite to that of integral shape dimension of pore surface on contribution rate, as shown in Figure 9. The fractal dimension of tortuosity is negatively correlated with surface diffusion contribution rate (k_B) and Knudsen diffusion contribution rate (k_N), and positively correlated with slip flow contribution rate (k_H). It comes down to the nature of fractal dimension. The larger the integral shape dimension of pore surface, the smaller the resistance of Knudsen diffusion and surface diffusion of gas molecules in shale porous media, and the greater the contribution of Knudsen diffusion and surface diffusion to apparent permeability. Although the contribution rate of slip flow decreases, the decrease is less than the total increase of Knudsen diffusion and surface diffusion, so the apparent permeability is higher. However, the larger the fractal dimension of tortuosity is, the more complex the pore structure is and the greater the diffusion resistance of gas molecules is. The contribution of Knudsen diffusion and surface diffusion to the apparent permeability decreases and the apparent permeability decreases.

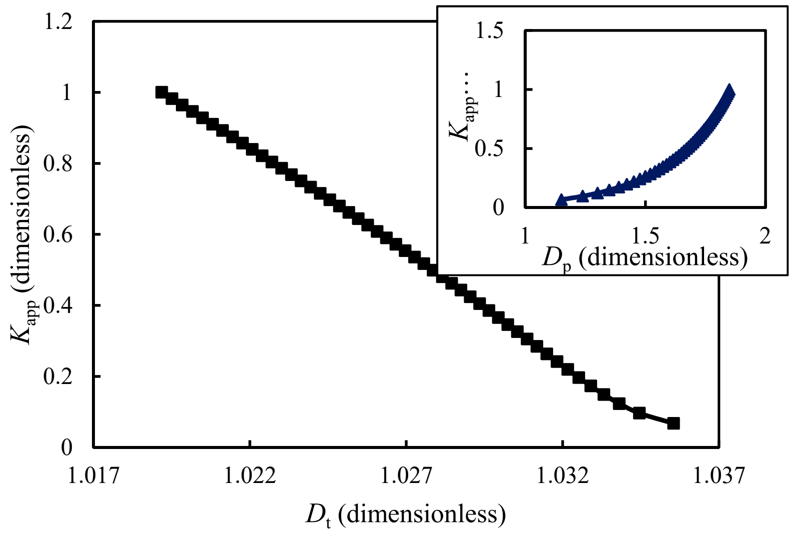

Figure 7. Effect of fractal dimension on dimensionless apparent permeability.

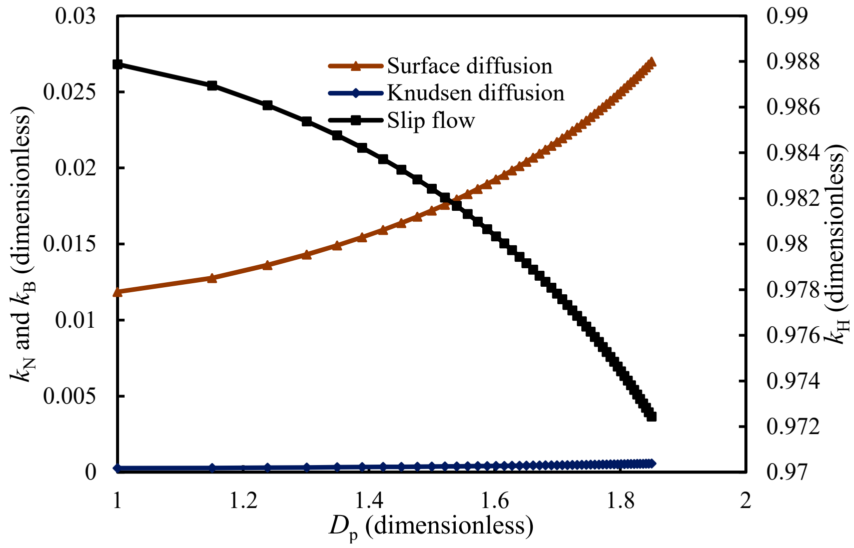

Figure 8. Relationship between contribution rate and fractal dimension of pore surface.

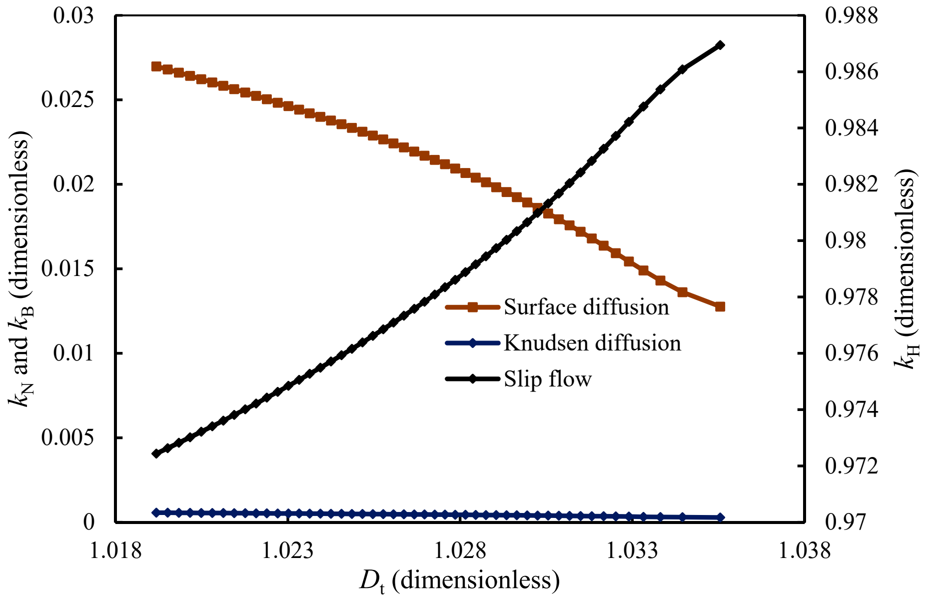

Figure 9. Relationship between contribution rate and fractal dimension of tortuosity.

5. Conclusions

In this paper, based on fractal geometry theory, the Hagen Poiseuille law, the Langmuir adsorption law, and Darcy law, a mathematical model of gas flow in nano-pores of shale was established. A new shale apparent permeability model is derived. The model comprehensively considers the influence of slip flow, Knudsen diffusion and surface diffusion, and is closely related to the size parameters of shale nano-pore structure, which can better reveal the behavior and law of multi-scale gas nonlinear flow in shale reservoir than traditional models. The nonlinear flow law of shale gas and the influencing factors of shale apparent permeability are analyzed. The following conclusions and understandings are obtained:

(1) The smaller the pressure, the higher the temperature, the larger the integral dimension of pore surface, the smaller the fractal dimension of tortuosity, the larger the apparent permeability, and the stronger the nonlinear flow of shale gas.

(2) The apparent permeability changes rapidly when the pressure is less than 10 MPa, and slowly when the pressure exceeds 10 MPa. Under any conditions, the contribution of slip flow to apparent permeability is the largest, followed by surface diffusion and Knudsen diffusion. The contribution rate of slip flow to apparent permeability increases rapidly and then tends to flatten with the increase of pressure, while the contribution rate of surface diffusion to apparent permeability decreases rapidly and then tends to flatten with the increase of pressure. Surface diffusion contributes significantly to apparent permeability at low pressure. The contribution of slip flow to the apparent permeability is dominant, while the contribution of Knudsen diffusion to the apparent permeability is small, which can be ignored.

(3) Fractal dimension of pore surface is positively correlated with apparent permeability, surface diffusion and Knudsen diffusion. The fractal dimension of tortuosity is negatively correlated with apparent permeability, surface diffusion and Knudsen diffusion. The fractal dimension of pore surface and the fractal dimension of tortuosity have the opposite effect on gas flow of shale nano-pores.

Author Contributions: Q.W. and J.Z. (Jinzhou Zhao) deduced the formula, verified the results and analyzed the influencing factors. Y.H. and L.R. provided validation data and examined the format and grammar of the paper. C.Z. and J.Z. (Jin Zhao) revised the manuscript for submission.

Funding: The authors would like to acknowledge the financial support of the National Natural Science Foundation of China (51404204); the National Science and Technology Major Project of the Ministry of Science and Technology of China (2016ZX05060).

Conflicts of Interest: The authors declare no conflict of interest.

References

1. Nguyen, V.H.; Rohan, E.; Naili, S. Multiscale simulation of acoustic waves in homogenized heterogeneous porous media with low and high permeability contrasts. *Int. J. Eng. Sci.* **2016**, *101*, 92–109. [CrossRef]
2. Pia, G.; Sanna, U. An intermingled fractal units model and method to predict permeability in porous rock. *Int. J. Eng. Sci.* **2014**, *75*, 31–39. [CrossRef]
3. Kuuskraa, V.A.; Wicks, D.E.; Thruber, J.L. Geologic and reservoir mechanisms controlling gas recovery from the Antrim shale. In Proceedings of the SPE Annual Technical Conference and Exhibition, Washington, DC, USA, 4–7 October 1992. Paper SPE 24883.
4. Roy, S.; Raju, R. Modeling gas flow through microchannels and nanopores. *J. Appl. Phys.* **2003**, *93*, 4870–4878. [CrossRef]
5. Javadpour, F. Nanopores and apparent permeability of gas flow in mudrocks (shales and siltstone). *J. Gas Can. Pet. Technol.* **2009**, *48*, 16–21. [CrossRef]
6. Freeman, C.M. A numerical study of microscale flow behavior in tight gas and shale gas. In Proceedings of the SPE Annual Technical Conference, Florence, Italy, 19–22 September 2010. Paper SPE 141125.
7. Curtis, M.E.; Ambrose, R.J.; Sondergeld, C.H. Structural characterization of gas shales on the micro- and nano-scales. In Proceedings of the Canadian Unconventional Resources and International Petroleum Conference, Calgary, AB, Canada, 19–21 October 2010; Paper SPE 137693.
8. Ebrahim, F.I.; Yucel, A. Lattice Boltzmann method for simulation of shale gas transport in kerogen. In Proceedings of the SPE Annual Technical Conference, Denver, CO, USA, 30 October–2 November 2011; Paper SPE 146821.
9. Shabro, V.; Torres-Verdin, C.; Javadpour, F. Numerical simulation of shale-gas production: From pore-scale modeling of slip-flow, Knudsen diffusion, and Langrnuir desorption to reservoir modeling of compressible fluid. In Proceedings of the North American Unconventional Gas Conference, Woodlands, TX, USA, 14–16 June 2011; Paper SPE 144355.
10. Michel, G.G.; Sigal, R.F.; Civan, F.; Devegowda, D. Parametric investigation of shale gas production considering nano-scale pore size distribution, formation factor, and non-darcy flow mechanisms. In Proceedings of the SPE Annual Technical Conference, Denver, CO, USA, 30 October–2 November 2011; Paper SPE 147438.
11. Freeman, C.M.; Moridis, G.J.; Michael, G.E. Measurement modeling, and diagnostics of flowing gas composition changes in shale gas wells. In Proceedings of the SPE Latin America and Caribbean Petroleum Engineering Conference, Mexico City, Mexico, 16–18 April 2012; Paper SPE 153391.
12. Javadpour, F.; Fisher, D.; Unsworth, M. Nanoscale gas flow in shale gas sediments. *J. Gas Can. Pet. Technol.* **2007**, *46*, 55–61. [CrossRef]
13. Swami, V.; Settari, A. A pore scale gas flow model for shale gas reservoir. In Proceedings of the Americas Unconventional Resources Conference, Pittsburgh, PA, USA, 5–7 June 2012; Paper SPE 155756.
14. Guo, C.H.; Bai, B.J.; Wei, M.Z.; He, X.; Wu, Y.S. Study on gas permeability in nano-pores of shale gas reservoirs. In Proceedings of the SPE Unconventional Resources Conference Canada, Calgary, AB, Canada, 5–7 November 2013; Paper SPE 167179.
15. Singh, H.; Javadpour, F.; Ettehadtavakkol, A. Nonempirical apparent permeability of shale. *SPE Reserv. Eval. Eng.* **2013**, *7*, 414–424. [CrossRef]
16. Mohammad, K.; Ali, T.B. An analytical model for shale gas permeability. *Int. J. Coal Geol.* **2015**, *146*, 188–197.
17. Zhang, L.; Li, D.; Lu, D.; Zhang, T. A new formulation of apparent permeability for gas transport in shale. *J. Nat. Gas Sci. Eng.* **2015**, *23*, 221–226. [CrossRef]
18. Wang, J.; Liu, H.Q.; Wang, L.; Zhang, H.; Luo, H.; Gao, Y. Apparent permeability for gas transport in nanopores of organic shale reservoirs including multiple effects. *Int. J. Coal Geol.* **2015**, *152*, 50–62. [CrossRef]
19. Wu, K.; Chen, Z.X.; Li, X.F.; Guo, C.; Wei, M. A model for multiple transport mechanisms through nanopores of shale gas reservoirs with real gas effect-adsorption-mechanic coupling. *Int. J. Heat Mass Transf.* **2016**, *93*, 408–426. [CrossRef]
20. Wang, J.; Kang, Q.; Wang, Y.; Pawar, R.; Rahman, S.S. Simulation of gas flow in micro-porous media with the regularized lattice Boltzmann method. *Fuel* **2017**, *205*, 232–246. [CrossRef]

21. Wang, S.; Shi, J.; Wang, K.; Sun, Z.; Miao, Y.; Hou, C. Apparent permeability model for gas transport in shale reservoirs with nanoscale porous media. *J. Nat. Gas Sci. Eng.* **2018**, *55*, 508–519. [CrossRef]
22. Zhang, T.; Li, X.; Shi, J.; Sun, Z.; Yin, Y.; Wu, K.; Li, J.; Feng, D. An apparent liquid permeability model of dual-wettability nanoporous media: A case study of shale. *Chem. Eng. Sci.* **2018**, *187*, 280–291. [CrossRef]
23. Li, C.; Lin, M.; Ji, L.; Jiang, W.; Cao, G. Rapid evaluation of the permeability of organic-rich shale using the 3D intermingled-fractal model. *SPE J.* **2018**, *23*, 2175–2187. [CrossRef]
24. Shen, Y.; Li, C.; Ge, H.; Guo, X.; Wang, S. Spontaneous imbibition process in micro-nano fractal capillaries considering slip flow. *Fractals* **2017**, *26*, 184002. [CrossRef]
25. Lee, J.W.; Nilson, R.H.; Templeton, J.A.; Griffiths, S.K.; Kung, A.; Wong, B.M. Comparison of Molecular Dynamics with Classical Density Functional and Poisson–Boltzmann Theories of the Electric Double Layer in Nanochannels. *J. Chem. Theory Comput.* **2012**, *8*, 2012–2022. [CrossRef] [PubMed]
26. Shen, Y.; Pang, Y.; Shen, Z.; Tian, Y.; Ge, H. Multiparameter analysis of gas transport phenomena in shale gas reservoirs: Apparent permeability characterization. *Sci. Rep.* **2018**, *8*, 2601. [CrossRef]
27. Miao, T.; Chen, A.; Zhang, L.; Yu, B. A novel fractal model for permeability of damaged tree-like branching networks. *Int. J. Heat Mass Transf.* **2018**, *127*, 278–285. [CrossRef]
28. Takbiri-Borujeni, A.; Fathi, E.; Kazemi, M.; Belyadi, F. An integrated multiscale model for gas storage and transport in shale reservoirs. *Fuel* **2019**, *237*, 1228–1243. [CrossRef]
29. Tan, X.H.; Liu, J.Y.; Li, X.P.; Zhang, L.H.; Cai, J.C. A simulation method for permeability of porous media based on multiple fractal model. *Int. J. Eng. Sci.* **2015**, *95*, 76–84. [CrossRef]
30. Hosa, A.; Curtis, A.; Wood, R. Calibrating Lattice Boltzmann flow simulations and estimating uncertainty in the permeability of complex porous media. *Adv. Water Resour.* **2016**, *94*, 60–74. [CrossRef]
31. Zhao, J.; Wang, Q.; Hu, Y.; Ren, L.; Zhao, C. Numerical investigation of shut-in time on stress evolution and tight oil production. *J. Pet. Sci. Eng.* **2019**, *179*, 716–733. [CrossRef]
32. Chalmers, G.R.; Bustin, R.M.; Power, I.M. Characterization of gas shale pore systems by porosimetry, pycnometry, surface area, and field emission scanning electron microscopy/transmission electron microscopy image analyses: Examples from the Barnett, Woodford, Haynesville, Marcellus, and Doig units. *AAPG Bull.* **2012**, *96*, 1099–1119.
33. Wang, F.; Zhao, J. A mathematical model for co-current spontaneous water imbibition into oil-saturated tight sandstone: Upscaling from pore-scale to core-scale with fractal approach. *J. Pet. Sci. Eng.* **2019**, *178*, 376–388. [CrossRef]
34. Su, P.; Xia, Z.; Qu, L.; Yu, W.; Wang, P.; Li, D.; Kong, X. Fractal characteristics of low-permeability gas sandstones based on a new model for mercury intrusion porosimetry. *J. Nat. Gas Sci. Eng.* **2018**, *60*, 246–255. [CrossRef]
35. Yu, B.; Lee, L.; Cao, H. Fractal characters of pore microstructures of textile fabrics. *Fractals* **2001**, *9*, 155–163. [CrossRef]
36. Wu, J.S. *Analysis of Resistance for Flow through Porous Media*; Zhejiang University: Hangzhou, China, 2006.
37. Chen, Z.L.; Wang, N.T.; Sun, L.; Tan, X.H.; Deng, S. Prediction method for permeability of porous media with tortuosity effect based on an intermingled fractal units model. *Int. J. Eng. Sci.* **2017**, *121*, 83–90. [CrossRef]
38. Zhao, J.; Zhao, J.Z.; Hu, Y.Q.; Zhao, C.N.; Wang, Q.; Zhao, X.; Zhang, Y. Coiled tubing friction reduction of plug milling in long horizontal well with vibratory tool. *J. Pet. Sci. Eng.* **2019**, *177*, 452–465.
39. Yu, B.; Li, J. Some characters of porous media. *Fractals* **2011**, *8*, 365–372.
40. Fan, W.; Sun, H.; Yao, J.; Fan, D.; Zhang, K. A new fractal transport model of shale gas reservoirs considering multiple gas transport mechanisms, multi-scale and heterogeneity. *Fractals* **2018**, *26*, 1850096. [CrossRef]
41. Sun, Z.; Shi, J.; Wu, K.; Zhang, T.; Feng, D.; Huang, L.; Shi, Y.; Ramachandran, H.; Li, X. An analytical model for gas transport through elliptical nanopores. *Chem. Eng. Sci.* **2019**, *199*, 199–209. [CrossRef]
42. Wu, K.; Li, X.F.; Wang, C.C.; Chen, Z.; Yu, W. Apparent permeability for gas flow in shale reservoirs coupling effects of gas diffusion and desorption. In Proceedings of the Unconventional Resources Technology Conference, Denver, CO, USA, 25–27 August 2014. Paper SPE 1921039.
43. Wu, K.; Li, X.; Wang, C.; Chen, Z.; Yu, W. A model for gas transport in microfractures of shale and tight gas reservoirs. *AIChE J.* **2015**, *61*, 2079–2088. [CrossRef]
44. Wu, K.; Chen, Z.X.; Li, X.F. Real gas transport through nanopores of varying cross-section type and shape in shale gas reservoirs. *Chem. Eng. J.* **2015**, *281*, 813–825. [CrossRef]

45. Chen, Y.D.; Yang, R.T. Concentration dependence of surface diffusion and zeolitic diffusion. *AIChE J.* **1991**, *37*, 1579–1582. [CrossRef]
46. Letham, E.A. *Matrix Permeability Measurements of Gas Shales: Gas Slippage and Adsorption as Sources of Systematic Error*; University of British Columbia: Vancouver, BC, Canada, 2011.
47. Song, W.; Yao, J.; Li, Y.; Sun, H.; Zhang, L.; Yang, Y.; Zhao, J.; Sui, H. Apparent gas permeability in an organic-rich shale reservoir. *Fuel* **2016**, *181*, 973–984. [CrossRef]
48. Wang, J.; Luo, H.; Liu, H.; Cao, F.; Li, Z.; Sepehrnoori, K. An integrative model to simulate gas transport and production coupled with gas adsorption, non-Darcy flow, surface diffusion, and stress dependence in organic-shale reservoirs. *SPE J.* **2017**, *22*, 244–264. [CrossRef]
49. Wang, S.; Tao, W.U.; Cao, X.; Zheng, Q.; Ai, M. A fractal model for gas apparent permeability in microfracture of tight/shale reservoirs. *Fractals* **2017**, *25*, 1750036. [CrossRef]
50. Sun, Z.; Li, X.; Shi, J.; Zhang, T.; Sun, F. Apparent permeability model for real gas transport through shale gas reservoirs considering water distribution characteristic. *Int. J. Heat Mass Tran.* **2017**, *115*, 1008–1019. [CrossRef]
51. Civan, F. Effective correlation of apparent gas permeability in low-permeability porous media. *Transp. Porous Media* **2010**, *82*, 375–384. [CrossRef]